A Computational Tool for Pre-operative Breast Augmentation Planning in Aesthetic Plastic Surgery

Joachim Georgii, Maximilian Eder, Kai Bürger, Sebastian Klotz, Florian Ferstl,
Laszlo Kovacs and Rüdiger Westermann

***Abstract*—Breast augmentation was the most commonly performed cosmetic surgery procedure in 2011 in the United States. Although aesthetically pleasing surgical results can only be achieved if the correct breast implant is selected from a large variety of different prosthesis sizes and shapes available on the market, surgeons still rely on visual assessment and other subjective approaches for operative planning because of lacking objective evaluation tools.**

In this paper we present the development of a software prototype for augmentation mammaplasty simulation solely based on 3D surface scans, from which patient-specific finite element models are generated in a semi-automatic process. The finite element model is used to pre-operatively simulate the expected breast shapes using physical soft tissue mechanics. Our approach uses a novel mechanism based on so-called displacement templates, which, for a specific implant shape and position, describe the respective internal body forces. Due to a highly efficient numerical solver we can provide immediate visual feedback of the simulation results, and thus the software prototype can be integrated smoothly into the medical workflow. The clinical value of the developed 3D computational tool for aesthetic breast augmentation surgery planning is demonstrated in patient-specific use cases.

***Index Terms*—Breast augmentation, Implant Simulation, Finite Elemente Simulation, Surgical Planning**

I. Introduction

Breast augmentation was the most commonly performed cosmetic surgery procedure in 2011 with 307,180 women in the United States undergoing augmentation mammaplasty with inserted implants under or in front of the pectoral muscle, a 45% increase from 2000 [1], [2]. Although correct breast implant selection defines the aesthetically pleasing surgical result and a large variety of different prosthesis sizes and shapes are available on the market, surgeons still rely on visual assessment and other subjective approaches for operative planning because of lacking objective evaluation tools [3], [4]. Classical methods for breast augmentation planning and implant selection as ordinary 2D digital photography [5], anthropomorphic evaluations [6], water displacement [7], plaster casting [8], radiological assessments [9], [10], [11], volume measurement devices [12], [13] and the commonly performed method of placing varying implant sizes in the patients bras to select the proper prosthesis [14] are subjective, observer dependant, unreliable, cumbersome, time consuming, cost intensive and and mostly of limited help for the surgeon [4], [15], [16], [17], [18].

Plastic surgeons could benefit from objective tools to measure and predict the aspired post-operative three-dimensional (3D) changes of the breasts after augmentation mammaplasty [19], [20], [21]. 3D quantification of the breast region using magnetic resonance imaging (MRI) or computed tomography (CT) provides accurate breast volume calculation and enables precise anatomical 3D reconstruction for numerical soft-tissue deformation simulation [16], [17], [18], [19], [22]. However, MRI/CT are expensive, time consuming, and the costs are not reimbursed by health insurance companies because of a lack of clinical prognosis for these examinations in aesthetic surgeries and in case of CT the patient is furthermore exposed to radiation. Furthermore, soft-tissue deformations or compressions are caused by the supine or prone patient positioning during acquisition which do not allow objective 3D evaluation of the real breast contour [10], [11], [19]. In addition, patients' acceptance for tomography imaging is limited because of serious noise exposure, potential claustrophobia and the necessity not to move during assessment hinder a routine 3D patient data acquisition in plastic and aesthetic surgery using MRI/CT [19].

Because of the limitations of the above named classical methods in breast augmentation planning, different 3D surface imaging systems (laser scan, stereophotogrammetry, fringe light projection etc.) were developed and several studies demonstrated the clinical value of 3D surface imaging as a non-invasive, reliable, precise, accurate and objective method to pre- and postoperatively evaluate 3D breast morphology in augmentation mammaplasty [4], [19], [23], [24], [25], [26]. Further studies presented 3D morphing systems to virtually deform and model the patients 3D surface breast shape [27], [28], [29]. The commercially available 3D imaging systems and software solutions like Precision Light, Inc. (Los Gatos, California, USA), 3dMD (Atlanta, Georgia, USA), Axis Three (Boston, Massachusetts, USA) and Canfield Scientific, Inc. (Fairfield, New Jersey, USA) do not take the biomechanical soft-tissue behavior into account, suffer from a lack of sufficient clinical validation and are therefore currently limited for breast augmentation simulation [29]. Computational modeling of soft tissue mechanics solely based on 3D surface scans showed promising results, but a specific description of the used 3D breast model and the applied numerical algorithms

K. Bürger, F. Ferstl, S. Klotz and R. Westermann are with the Computer Graphics & Visualization Group, Technische Universität München, Germany. Email: buerger@tum.de, florian.ferstl@tum.de, klotz@in.tum.de, westermann@tum.de.

M. Eder and L. Kovacs are with the research group CAPS - Computer Aided Plastic Surgery, Department of Plastic Surgery and Hand Surgery, Klinkum rechts der Isar, Technische Universität München, Germany. Email: m.eder@caps.me.tum.de, l.kovacs@lrz.tum.de.

J. Georgii is with Fraunhofer MEVIS, Institute for Medical Image Computing, Bremen, Germany. Email: Joachim.Georgii@mevis.fraunhofer.de.

to simulate breast implant and soft-tissue interactions for augmentation mammaplasty are still required [30], [31], [32]. Recent work presents implant simulation using Finite Element (FE) models based on CT images, which, however, limits the application due to the required radiation exposure and computation time [33]. Currently, 3D surface imaging is also limited for a reliable generation of a closed 3D breast model because no rear boundary of the thoracic wall is technically ascertainable [16], [17], [18].

A. Contribution

This study presents the development of a software prototype for augmentation mammaplasty simulation solely based on 3D surface scans. It is based on patient-specific finite element models, which are generated in a semi-automatic process from the surface scans using a standardized workflow. The finite element model is used to pre-operatively simulate the expected breast shapes using physical soft tissue mechanics. A highly efficient numerical solver allows reducing waiting times significantly, providing immediate visual feedback of the simulation results. Due to the intuitive semi-automatic model generation process as well as the high performance of the simulation method, the software prototype can be integrated smoothly into the medical workflow regardless which kind of 3D imaging device (laser scan, stereophotogrammetry, fringe light projection etc.) is applied. The clinical value of the developed 3D computational tool for aesthetic breast augmentation surgery planning is demonstrated in patient-specific use cases.

The proposed prototype comes along with a number of technological challenges that have to be addressed in order to allow for an accurate, yet interactive breast augmentation simulation. The first challenge is the semi-automatic construction of a closed finite-element model from a patient-specific open surface scan. We provide a solution that only requires the specification of few anatomical landmarks and computes a closed breast volume from these landmarks automatically. The second challenge is the efficient simulation of the implant insertion and the deformation that is caused by the insertion into the breast. Our approach uses a novel mechanism based on so-called displacement templates, which, for a specific implant shape and position, describe the internal body forces this implant would cause. The corresponding positional changes are then fed into a finite element solver to compute the resulting deformation. By means of this approach, the use of a geometric implant model, and in particular the complicated simulation of the two-way coupling between the implant and the enclosing breast can be avoided. The third challenge is to give the user full interactive control over implant placement and shape. We address this requirement in two ways: First, we propose an intuitive mechanism to place a selected implant in the breast volume and provide few intuitive parameters to control the implant's shape. Second, we consider performance issues throughout the entire pipeline and tightly couple simulation and visualization to enable immediate visual feedback. Therefore, the optimal placement and shape of a selected implant type can be intuitively determined.

II. Method Overview

In this section we give an overview of the pre-operative 3D planning tool developed. It is based on patient-specific 3D surface scans, which are acquired by a 3D laser scanner system. These surface meshes can then be loaded in our software prototype, where we developed and implemented a pipeline to semi-automatically process the data to obtain a patient-specific finite element model. This pipeline is illustrated in Figure 1.

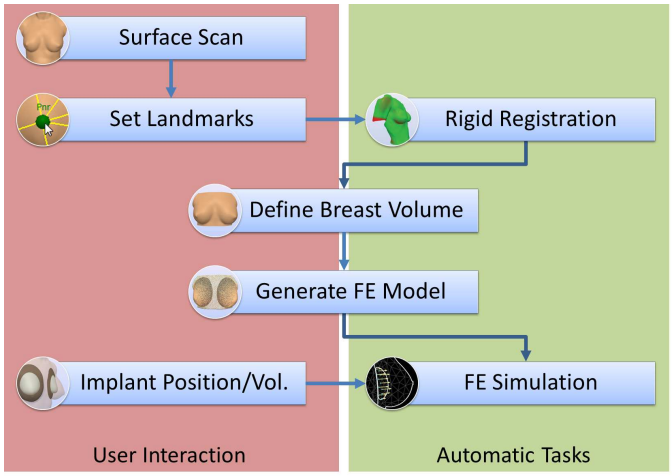

Fig. 1. Overview of the proposed system for breast augmentation simulation.

The first step is to set well-defined anatomical landmarks on the 3D surface scan. These landmarks are required to define and measure the breast contour and to quantify differences between pre- and post-operative scans. The next major step is to reconstruct the back wall (rear demarcation of the chest wall) for the breast models. The chest wall is needed to generate a closed surface mesh from which a volumetric simulation model can be computed. Furthermore, the back wall is used to place selected implants anatomically correct in the simulation process. The region of each breast is defined in an interactive session, and the surface scan is cut at the region boundaries into three parts—the left and right breast, and the body part. The left and right breasts are cut out of the surface scan and the emerging holes are closed by taking into account the curvature of the surrounding parts. This process generates the body mesh, and it is discussed in Section IV-C in detail. To only spend the degrees of freedom in the anatomical region of interest, i.e. the breast and the surrounding of the implant, the original 3D scan and the body mesh are additionally cut by pre-defined planes (left, right, top and bottom), and the resulting meshes are connected to construct a closed surface mesh. This mesh defines the volume in which the tissue is simulated using a finite element method. Figure 4 depicts all major steps which are performed to generate the closed surface mesh.

The closed surface mesh is finally triangulated to generate a tetrahedral volumetric finite element model. To accelerate the simulation procedure, we use a hierarchical representation of the finite element model. Therefore, we use a triangulation algorithm, which can be parameterized to generate ever coarser simulation models. The simulation uses a geometric multigrid

solver to solve the static elasticity problem very efficiently [34], [35]. It can accurately handle large strain deformations and allows fast updates due to its implicit nature. The details of the computational simulation machinery are described in Section V.

III. 3D Data Acquisition

3D breast surface scans of female patients undergoing breast augmentation with silicone implants were obtained before and 6 months after surgery using a 3D surface laser scanner (Vivid 910®, Konica-Minolta Co, Osaka, Japan) according to a standardized and previously reported 3D acquisition protocol [16], [17], [18], [21]. The scanner was placed 1.5 meters from the subject and the region between the jugulum and the navel was assessed with the scanner in 10 degrees upward position in approximately 1.5 seconds. Three single scans were obtained from a standing position on predefined markers on the ground with the subject facing +30, 0 and -30 degrees relative to the lens [36]. The patients hold their breath during acquisition with arms down the side crossed behind at the height of the pelvis and the patients back supported by a wall to guarantee reproducible data [23], [24].

All shots were carried out under standardized lighting conditions with room light of an intensity ranging between 350 and 400 lux. The scanner is based on the principal of laser triangulation and the object is detected by a plane of laser light coming from the source aperture of the scanner and is swept across the detected region by a mirror, rotated by a galvanometer. Each laser light stripe is reflected from the subject surface and acquired by a CCD camera. The surface contour measurements of the subject are obtained through triangulation from each reflected scan line and converted into a 3D polygon mesh (around 150.000 points). Using middle lens with focal length distance f = 14 mm, the scanner captures 198 to 823 mm in X direction, 148 to 618 mm in Y, and 70 to 800 mm in Z with an acquisition accuracy up to 0.10 mm to the reference plane. The captured three single scans were converted into one single virtual 3D model using appropriate software (Raindrop Geomagic Studio 11®, Raindrop Geomagic, Inc., NC, USA) that detects corresponding parts in overlapping regions.

IV. Generation of a Patient-Specific 3D Breast Model from Surface Scans

The 3D laser scanner provides high-resolution surface meshes, from which volumetric finite element models are constructed in a semi-automatic process. This process is controlled via a planning tool that allows selecting the specific breast region to be augmented and simulating the insertion of different kinds of implants into this region. The tool also provides easy-to-use measurement functionality to analyze the differences between the real surgical outcome and the simulated post-operative result.

A. Anatomical Landmarks

Anatomical landmarks can be positioned interactively on the patient's surface scan, and they are used throughout the whole data processing pipeline. Landmark placement is performed by rendering the surface scan and determining the triangle—given by a unique id—below the mouse cursor. From the cursor position in screen space the exact landmark position in 3D can then be computed and used to render a small sphere at this position. Figure 2 shows the set of pre-defined landmarks which must be placed by the user to enable an automatic realization of the following task:

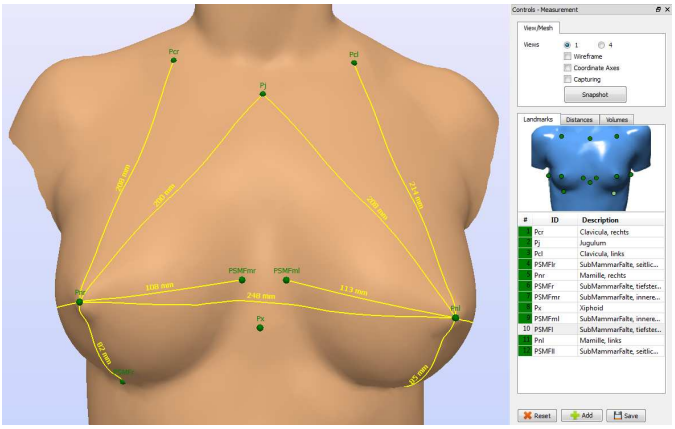

Fig. 2. Anatomical landmarks and distances used by the planning tool. Landmarks: Pcl = clavicle left, Pcr = clavicle right, Pj = sternal notch, Pnr = nipple right, Pnl = nipple left, PSMFr = lowest point of the submammary fold right, PSMFl = lowest point of the submammary fold left, PSMFmr = medial border of the submammary fold right, PSMFml = medial border of the submammary fold left, PSMFlr = lateral border of the submammary fold right, PSMFll = lateral border of the submammary fold left, Px xiphoid.

- **Measurement**: Distances between landmarks are used to quantify differences or asymmetries on the surface scan and to evaluate the surgical outcome [23], [24], [25], [26]. (The clinically most relevant distances on both sides between specific landmarks are the following: Pc to Pn, Pj to Pn, Pn to PSMF, Pn to PSMFm, Pn to PSMFl, Pnl to Pnr, see Figure 2.) The planning tool supports measurements on the breast surface (on-surface distances) as well as Euclidean distances. To compute on-surface distances between two landmarks, approximate geodesic distances are used. Therefore, the plane passing through the two landmarks and being orthogonal to the coronal plane is intersected with the surface, and the length of

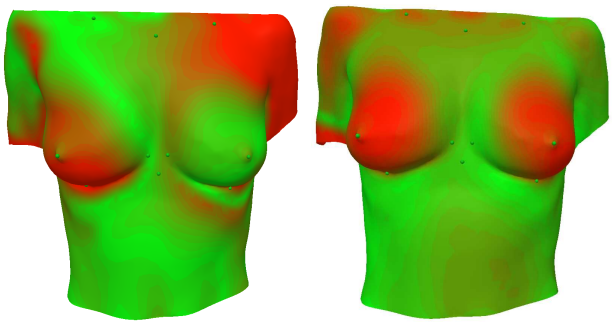

Fig. 3. Rigid registration of two surface scans is performed automatically after the anatomical landmarks have been set. Left: Distances between a non-registered pair of pre- and post-operative surface scan are color coded (from green equals zero to red equals 20mm). Right: Distances between the automatically registered pair of surface scans.

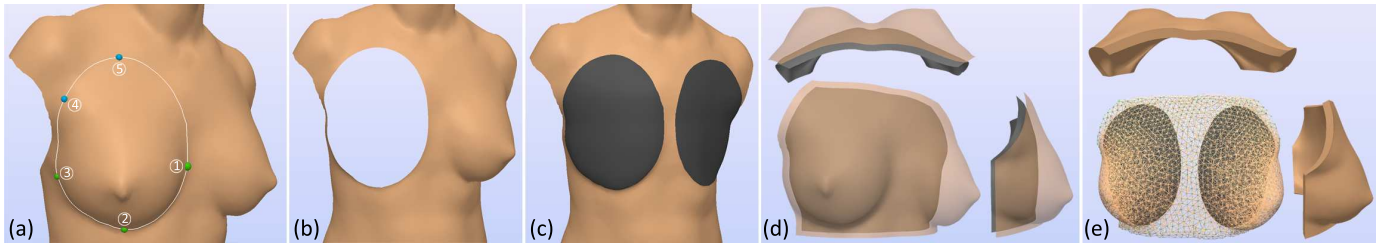

Fig. 4. Workflow for generating the volumetric breast model used in the FE simulation. (a) The breast region is segmented by a curve on the surface scan. The curve is generated by a set of control points, i.e. landmarks PSMFmr ①, PSMFr ②, PSMFlr ③, as well as two additional points on the surface (④, ⑤) that are computed automatically. (b) The mesh is cut along the curve, and the breasts are removed. (c) The resulting holes in the surface mesh are automatically filled, resulting in the rear wall. (d) Both the initial mesh and the rear wall are cut along planes (top, bottom. left, right) to reduce the simulation volume to the required region. The rear wall is shifted towards the back. (e) The meshes are connected at their boundary to define a closed surface representation.

the intersection curves is used as on-surface distance. The intersection curve is computed by tracing out this curve as described in the next subsection for generating a smooth curve passing through a set of landmarks.

- **Registration**: Different scans generated by the 3D laser scanner are not in the same coordinate system. In order to compare different scans of the same patient, i.e., the post- and pre-operative scans, surface meshes are first registered by means of the landmarks which are close to the bones and do not undergo soft tissue deformations during surgery (Pcl, Pcr, Pj and Px, see Figure 2). The registration is performed rigidly using principal component analysis. Figure 3 shows a post-operative scan before registration and after automatic registration to the pre-operative scan of the same patient.
- **Breast Volume**: From a set of pre-defined landmarks, the breast region is determined automatically according to the breast volume measurement protocol proposed in [17], [18], [23]. In this process, landmarks are used as control points in the construction of a smooth curve which segments the breast surface in the initial surface scan (see next Section for details).

In addition to the set of pre-defined landmarks which have to be specified to enable breast volume computation and construction of a volumetric breast model, the user can define additional landmarks and let distances between any pair of landmarks be computed automatically by the system.

B. Breast Volume

The planning tool automatically determines a first approximation of the breast region, i.e., the surface region which the surgeon considers as breast, from the pre-defined anatomical landmarks. This region is important for volume comparison between pre- and post-operative scans and for the construction of a volumetric breast model.

The breast region is defined via a curve on the initial surface scan—the so-called cut curve—which separates the breast. The curve is generated from a set of control points, i.e., the landmarks PSMFmr, PSMFr, PSMFlr as well as additional control points on the surface, which are automatically computed. Since the landmark Pcr is outside the breast region, we automatically determine a control point at a pre-defined ratio along the on-surface curve from Pcr to Pnr. An additional control point is inserted in the middle of the on-surface curve from this new control point to PSMFlr, since it is useful to adjust the automatically generated curve in the region of the armpit. An illustration of the separating curve as well as the control points used to construct this curve is given in Figure 4(a). The automatically computed curve can then be adjusted interactively by moving any of the control points on the mesh or arbitrarily inserting additional control points on the curve segments, thereby automatically performing the steps described in the following to compute the projected curve.

To compute the cut curve enclosing the breast, a closed sequence of 3D cubic Hermite splines is computed from the positions of the control points. At spline transitions, C^2 continuity is assured. Even though the 3D spline curve is enforced to pass through the specified control points on the surface, in general, it will not stay on the surface in between these points. Thus, in a second step the spline curve has to be projected onto the surface mesh to obtain the cut curve.

Projecting the spline curve onto the surface mesh is performed as follows: Starting with an arbitrary control point and the triangle containing it, a new point on the spline curve is computed using a pre-defined parameter increment. The line segment from the start point to the new point is then projected into the triangle plane using the triangle normal vector as the projection direction. If the projected line segment crosses one of the triangle edges, it is clipped at this edge and projected into the plane of the triangle adjacent across this edge. This process is repeated until the line's end point falls into the interior of a triangle, in which case a new sample point on the curve is taken and the process is repeated using the line from the current to this new point. All line-edge intersections and projected end points are stored in the order they are computed, giving the cut curve as a closed line strip which can be rendered on top of the surface.

C. Breast Model Construction

To obtain a volumetric breast model, a number of automatic steps are performed as illustrated in Figure 4(b)-(e). The basic idea is to use the cut curves to separate the breast surfaces from the initial surface scan, and then to compute smooth surfaces covering the resulting holes. These surfaces are then used to construct a closed rear wall which can be stitched to the initial surface scan.

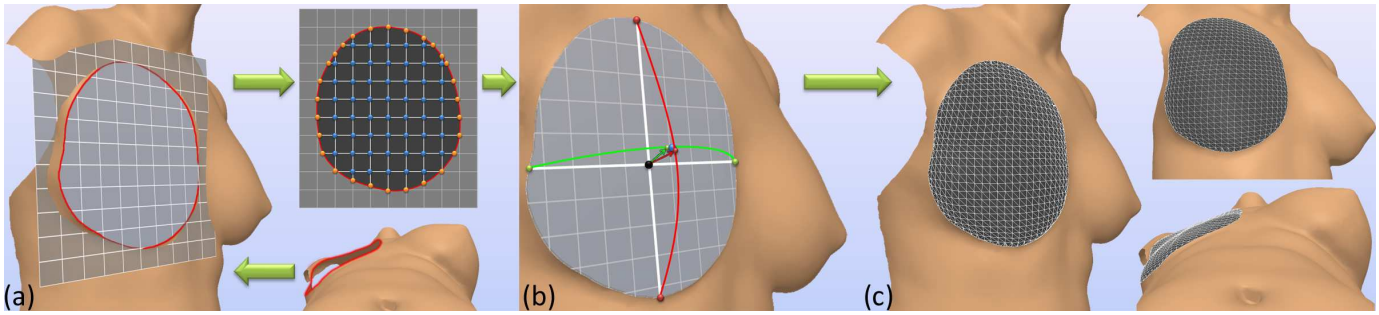

Fig. 5. Illustration of the approach to fill the holes in the base mesh after cutting out the breast. (a) A least-squares plane is fitted to the cut curve vertices, and these vertices are projected on the plane to generate a Delaunay triangulation using regularly distributed interior vertices (blue). (b) The obtained triangle mesh is smoothly adapted to the base mesh by averaging horizontal and vertical cubic Hermite splines. (c) The generated triangular fill-in mesh.

The cut curves are first constructed for the left and right breast as described (Figure 4(a)), and they are then used to cut the mesh into three disjoint parts—the left breast (LB), the right breast (RB), and the base (BS). Since the cut curve is projected onto the triangular surface mesh, generating these parts is straight forward: For each line segment of a cut curve, we locally cut the mesh by splitting the triangles the curve is passing through. Thus, the split triangle is replaced by two to three new triangles, which are assigned to the base and breast, respectively. If the curve is going exactly along a triangle edge, the two adjacent triangles are assigned unchanged. To decide which of the triangles belongs to the breast and which to the base mesh, we exploit the fact that the cut line is generated in a consistent ordering (defined by the anatomical landmarks). Therefore, we compute the signed distance of the triangle vertices opposite to the new edge to the plane defined by the line segment and the respective triangle normal. Depending on the sign, the triangles can then be assigned consistently. Figure 4(b) shows the resulting base mesh.

Now, a challenging step is to automatically fill the holes in the base mesh which occur when taking out LB and RB from BS. Filling these holes is important because the filled base serves as the rear wall in the following construction of a closed mesh representation. For each hole we generate one additional mesh—the left and right fill-in (LF,RF)—as follows. First, we project the boundaries of the holes (i.e. the cut curve) onto the regression plane of the curve points, which is computed via a least-squares method. We then compute a 2D Delaunay triangulation of the n-polygon defining the projected curve. However, in addition to the curve points we add additional points on a regular 2D lattice in the interior of the curve, and we let the Delaunay triangulation consider these points as well. This is illustrated in Figure 5 (a).

The reason for using additional points is that the fill-ins should not be planar but should smoothly extend the curved shape of the surrounding base surface. This is achieved by displacing the interior points according to a set of smoothly varying spline curves which are spanned over the interior part. In particular, for each of the rows and columns of the used lattice a 1D cubic Hermite spline is computed. The start and end points of each spline are the points on the cut curve where the respective rows and columns intersect this curve (see orange vertices in Figure 5(a)). The tangents of the base mesh at these points define the second pair of constraints for each spline (see Figure 5 (b)). Once the Hermite points and tangents are determined, the Hermite splines along the rows and columns can be evaluated at the parameter values corresponding to the positions of the lattice points. Each lattice point is set to the average between the positions of the spline curves along the rows and columns. A smooth fill-in that has been generated by the proposed method is shown in Figure 5 (c)). To further improve the smoothness of the reconstructed fill-ins, we apply a smoothing of the row and column tangents in advance, using a Gaussian filter of sufficient size. Finally, we apply 10 - 20 iteration steps of a Laplace Beltrami filter on the 3D triangular mesh to smooth it sufficiently.

As shown in Figure 4(c), the fill-ins are finally stitched together with the base BS in order to smoothly fill the holes. By using the initial surface scan including the breasts and the base with the fill-ins, we can now generate a volumetric model in a straight forward way. Therefore, we first clip both meshes at four appropriately selected planes to restrict the volume model to the relevant parts. The filled base is then shifted towards the back of the patient to account for the thickness of the skin and the muscle, such that the resulting back wall approximately has the niveau of the chest wall as shown in Figure 4(d). Finally, the clipped and shifted base and the clipped initial surface are connected along the boundaries via additional triangles so that a closed mesh is obtained. This mesh is shown in Figure 4(e).

The resulting closed mesh is then input to a 3D triangulation method which generates a volumetric tetrahedral mesh. We use the tetgen package [37] to construct a tetrahedralization, and we specify additional points in the interior of the mesh to guarantee a good aspect ratio of the elements. In particular, a Cartesian grid is overlaid with the surface mesh, and all grid points in the interior of the mesh are used as additional points. A beneficial side effect of this approach is that the resolution of the Cartesian grid can be varied in order to generate a hierarchy of tetrahedral grids at ever coarser resolution. We use the quality parameters of tetgen, and by doing so the surface mesh is also re-meshed appropriately at the coarser levels. The hierarchy generated in this way is required by the geometric multigrid solver which we use to simulate the implant insertion efficiently (see Section V).

V. Simulation

The simulation approach we use for estimating the breast deformations due to the insertion of an implant is based on the corotational formulation of elasticity. The approach works on a finite element discretization of the breast using tetrahedral elements. Breast deformations are described as a mapping from the breast's reference configuration Ω to its deformed configuration $\{x + u(x) \mid x \in \Omega\}$ using a displacement function $u : \mathbb{R}^3 \rightarrow \mathbb{R}^3$. The displacement function specifies for every grid vertex the movement of this vertex due to internal and external forces.

The dynamic behavior of an elastic object is governed by the Lagrangian equation of motion

$$M\ddot{u} + C\dot{u} + Ku = f, \tag{1}$$

where M, C, and K denote the mass, damping and stiffness matrices. u is a vector built from the displacement vectors of all vertices and analogously, f is constructed from the vertex force vectors, i.e., external forces and body forces such as gravity. The stiffness matrix K is build by assembling the element stiffness matrices K_e, which are determined from the formulation of the strain tensor and the material law. To keep the matrices K_e linear with respect to u, we apply the Cauchy strain formulation together with the generalized Hooke's law, yielding the formula $K_e = \int_{\Omega_e} B_e^{\mathrm{T}} D B_e \, dx$ with B_e being the element strain matrices. More details can be found in previous work on finite element methods [38], [39].

The Cauchy strain just gives a linear approximation of the full Green strain tensor and, thus, only yields a reasonably approximation for small deformations. To overcome this limitation we use the co-rotated Cauchy strain formulation [40] in our approach, which, in principle, rotates the elements from the deformed to the reference configuration before the linear strain approximation is computed. The element rotations are computed via the energy minimization approach by Georgii and Westermann [34].

To solve for the material displacements we use the implicit geometric multigrid solver proposed in [41], [35]. In a preprocess, the finite element discretizations are constructed at multiple resolutions as described in the previous section to obtain the grid hierarchy required by the solver. Due to the co-rotational formulation of strain, the equation systems at every level of the multigrid hierarchy have to be rebuilt in every simulation step before a typical multigrid V-cycle can be performed. In our current system, typical element numbers are in the range of 15K-60K, depending on the initial resolution of the surface scan. On a standard desktop computer, simulations on such meshes can be computed at times between 25ms-90ms per multigrid V(2,1)-cycle, enabling immediate visual feedback once an implant is inserted, re-positioned, or scaled in volume. Note that convergence of the solver is achieved after 3 to 5 V-cycles. We apply the deformation field computed at the finite element grid to the orginal surface scan by means of inter-/extrapolation thereby yielding visually pleasing results.

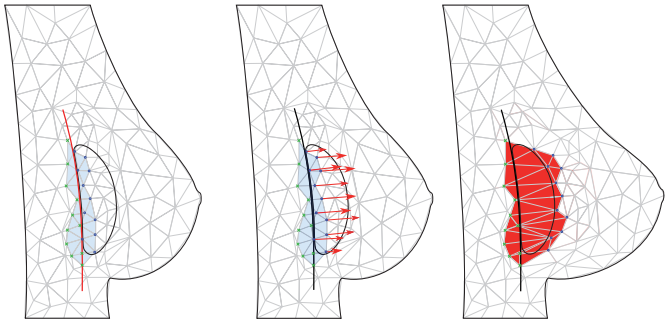

Fig. 6. Discrete implant simulation. Left: Vertices in front (blue) / back (green) of the implant surface are detected. Back vertices are fixed. Middle: To the front vertices, displacements are applied according to the projection (thickness) of the implant in normal direction of the implant surface. Right: Simulation result with discretized implant. Implant elements are denoted in blue (initial state) or red (deformed state).

A. Implant Simulation

To simulate the effect of an implant on the breast volume, in the current approach we assume the implant is a rigid body which is defined implicitly by a function describing its shape. Later in this text we will discuss the different shape functions provided by our tool.

To simulate the effects of these implants in an interactive environment, we do not cut the tetrahedral mesh of the breast to insert the implant as a separate object, since this involves time consuming recalculations of the finite element model and solver data structures. Instead, we blow up a thin region of the breast without modifying the tetrahedral mesh. We can illustrate the simulation approach by using an implant with a projection (thickness) equal to zero, which is inserted into the tetrahedral grid by finding the corresponding vertices of the tetrahedral mesh, and the tetrahedral grid is then deformed according to the implants effective projection at the respective mesh vertices. This procedure requires that we determine for each point of the implant surface its corresponding projection, i.e. the thickness of the implant.

The shape functions serve as displacement functions which describe the positional change of the breast tissue when an implant is inserted. In particular, given the shape function and the implant position, those vertices of the tetrahedral breast model that are covered by the implant can be determined procedurally, and they can then be displaced according to the displacement function so that they come to lie outside the implant. Such a displacement, which is only carried out for a thin shell of vertices, is illustrated in 2D in Figure 6. In the simulation process, the positions of the displaced vertices covered are considered as boundary constraints in the simulation, and the displacement of all other vertices is simulated accordingly.

To enable an accurate deformation simulation via displacement functions, we first adapt the finite element discretizations used in the elasticity simulation. In a pre-process, we determine the region in the interior of the breast which may be covered by an implant due to different positions and volumes. In this regions, additional vertices are inserted and the triangulation is refined using these vertices (see Figure 6

(left)). The refinement is necessary to allow for an accurate, discrete representation of the selected implant shape via the displaced vertices. This refinement is generated on the finest level of the multigrid hierarchy, and this hierarchy is generated by locally doubling the spacing of the interior, regularly distributed, vertices used in the meshing process.

In an interactive session, the user first selects a particular implant shape and volume, and positions this implant in the breast. Here, we use the slightly displaced fill-ins RF and LF (red curve in Figure 6) as surface models of the pectoralis muscle on top of which the implant is positioned. By using a specific point in the center of the implant's back wall—the so-called implant anchor point—positioning the implant means that this point is shifted along the fill-in and the implant is warped to the fill-in accordingly. Warping is implemented by adjusting the implicit implant functions described later to the local normals of the fill-in.

We first determine all tetrahedral elements intersecting the fill-in mesh using a kd-tree. For these so-called fill-in elements we denote all vertices in front of (anterior to) the fill-in mesh as front vertices; the vertices in back of (posterior to) the mesh are denoted as back vertices. We then use a Mercator projection to project the front / back vertices on the fill-in mesh yielding projected coordinates x' and y'. Given the fact that we describe the implant functions as a projection (thickness) value z over a 2D coordinate (x, y) as described in Section V-C, we can use the projected coordinates (x', y') to compute the implant thickness $z'(x', y')$ at that location. In case the implant thickness is greater than zero, the vertex is in the interior of the implant and is considered for further processing. In case the thickness is zero or undefined, the vertex is outside of the implant and thus ignored. An interior front vertex is denoted as implant vertex. In this case, we assume to displace the vertex in direction of the fill-ins normal accordingly to the implants thickness z'. In case of an interior back vertex, we set this vertex as fixed. Additionally, for all fill-in elements, we determine the set of elements that are incident to exclusively interior front / back vertices. For these so-called implant elements, we adjust the elastic modulus to a very soft material, and we set the density to the density of the implant (see Figure 6).

To finally compute the deformation of the breast, we partition the set of vertices into two subsets S_1 and S_2—the interior front/back vertices and the breast vertices—and we handle the respective vertices differently in the simulation. For the interior front/back vertices we use Dirichlet boundary conditions. This means that the displacements u_i of these vertices are given as constraints, and the respective forces to achieve these displacements are simulated. The forces acting on the breast vertices, on the other hand, are given (i.e. gravitation) and the respective displacements have to be simulated. We can thus split the linearized displacement and force vectors into u_1, f_1 and u_2, f_2, where u_1 and f_2 are known and f_1 and u_2 have to be computed. The system of equations to be solved in every simulation step can then be partitioned as

$$\begin{pmatrix} K_{11} & K_{12} \\ K_{21} & K_{22} \end{pmatrix} \begin{pmatrix} u_1 \\ u_2 \end{pmatrix} = \begin{pmatrix} f_1 \\ f_2 \end{pmatrix}.$$

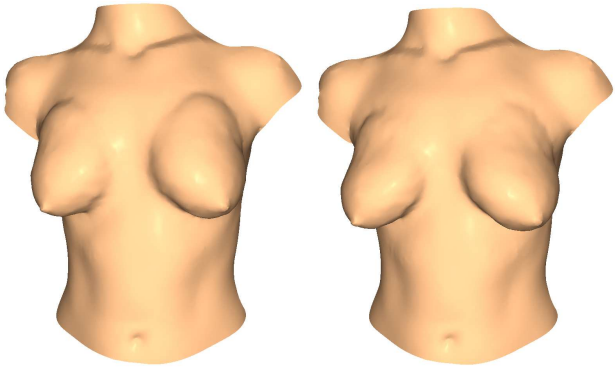

Fig. 7. Augmentation mammaplasty simulation without (left) and with (right) gravity correction for the inserted implant ($275\,\mathrm{cm}^3$ anatomic).

To embed this partitioning into the geometric multigrid solver we use the approach of elimination of the boundary conditions as proposed in [42].

B. Gravity Correction

By inserting the implant, the breast does not only increase in volume, but it also increases in mass due to the implant's mass which has not been considered so far. The initial surface scan was taken in standing position of the patient and, thus, it shows the breast shape under gravity. In the simulation so far, however, the effect of gravity on the implant was not considered, but it was inserted into the breast under gravity.

Since we simulate the implants by blowing up specific elements of the breast, we have to account for the mass increases and gravity effect of these elements. The general idea would be to determine the gravity free state of the breast, simulate the insertion of the implant and then simulate the effect of the gravity on the whole breast including the implant. Since the forces to switch to the gravity free state and back to the gravity state cancel for all but the implant elements, it is sufficient to only consider the implant elements. However, for performance reasons one will avoid to change the reference state (rest state) of the simulation, since this would require the stiffness matrices to be recomputed. Therefore, our goal is to include the effect of gravity of the inserted implant, which can be accounted for by determining the volume increase achieved by the implant. In order to do so, we cannot use Dirichlet boundary conditions for the implant, but we have to convert them into equivalent force constraints. Thus, we take the result of the implant simulation and convert it into pure force constraints, e.g. at the implant vertices the external forces

$$f_1 = K_{11}u_1 + K_{12}u_2,$$

are set, where u_1 and u_2 refer to the displacement which have been computed in the previous simulation step. Then, we run the simulation again without these Dirichlet boundary conditions but with the external forces at the implant vertices (and of course keeping the fixed vertices), and we add adjusted gravity forces for all implant elements that have be blown up. Taking into account that the initial finite element model is created in standing position of the patient, we only have to

take into account the gravity effect of the additional volume. We therefore use the deformed tetrahedral elements to compute the gravity contribution in the deformed state, and we subtract from it the gravity contribution of the initial rest state of the element. In that way, we get a gravity correction for each vertex of each implant element, which are assembled into a global gravity correction vector. Note, that the material parameters at these elements have already been updated. In this way, we simulate the effect of gravity of the introduced volume using the density of the implant introduced. Note that this additional simulation step can be performed very efficiently since we can use the displacement field of the initial simulation step as initial condition for the displacement field. Figure 7 gives an example of this gravity correction approach.

C. Predefined Implant Shapes

We distinguish between two kinds of implants in our simulation—round implants and anatomic implants. Round implants are defined by their diameter and projection, whereas anatomic implants are defined by width, height, and projection. Using these parameters, we derive analytical formulas to describe the implants surface in rest position—in the following we call this the *implant surface*.

To integrate implant simulation in our planning system, we define implicit functions which approximatively describe the shape of the implants available on the market, and which are controlled by the aforementioned parameters—width, height, and projection. This modeling approach has the advantage, that implants can be defined relatively simple by adapting parameters (we will introduce some more parameters that control the shape in this section). However, the alternative method to describe the implant shape by triangular meshes is more flexible in general, but additionally comes at higher computational costs at run time when the implants have to be simulated. This is due to the fact that the projection of the implant is not analytically given for an arbitrary surface point, but has to be determined by means of ray casting through the implant mesh. Since the focus of this work is to give immediate visual feedback, we focus on the first approximative approach.

1) Round Implants: Round implants can be approximated by 3D ellipsoids, which are bisected along their xy plane. To define the implicit function, we choose as parameters the diameter w and the projection p of the implant, where the latter one is associated with the local positive z axis. The surface of the implant is then defined as

$$\frac{x^2}{(w/2)^2} + \frac{y^2}{(w/2)^2} + \frac{z^2}{p^2} = 1 \ \wedge \ z > 0. \tag{2}$$

Therefore, the projection (or thickness) of the implant can be determined using the coordinates x and y:

$$z\left(x,y\right) = \left|\frac{p}{w}\right| \sqrt{w^2 - 4x^2 - 4y^2}. \tag{3}$$

By spatially varying the projection parameter p such that it reaches zero at the boundary of the implant we obtain a smoother transition at the implants boundary as illustrated in Figure 8:

$$p\left(x,y\right) = p \cdot \left(1 - 2\frac{x^2+y^2}{w^2}\right). \tag{4}$$

Fig. 8. Profile of the round implants (from bottom). Due to the adaption of $p(x,y)$, the profile can be varied slightly (right).

2) Anatomic Implants: The shape of anatomic implants are adapted to the shape of the female breast. We achieve this shape adaption in our implicit function by deforming a 3D ellipsoid. Since we have now an asymmetric shape, we need as parameters the width w, the height h as well as the projection p to describe the basic shape. To deform the ellipsoid, we perform two steps. First, we adapt the width of the implant in dependence of the local y coordinate, such that we achieve a diminution to the top. Second, we adapt the projection in dependence of the local x coordinate to change the profile of the implant accordingly.

For the first step, we choose the function

$$w\left(y\right) = w \cdot \left(\frac{-2\frac{y}{h} + a}{(a+1)\cdot b}\right), \tag{5}$$

where parameters a and b are used to control the shape of the diminution. In our examples, we choose two different sets of parameters, one for implants with large heights ($a = 3$, $b = 0.78$, see Figure 9 left) and one for implants with small height ($a = 10$, $b = 0.91$).

For the second step, we define the projection as the

$$p\left(x,y\right) = p\ \psi(x)\ \chi(y), \tag{6}$$

where $\psi\left(x\right)$ adapts the projection with respect to the local x axis, and $\chi\left(y\right)$ adapts the projection with respect to the height as illustrated in Figure 9 (right):

$$\psi\left(x\right) \ = \ 1 - 2\left(\frac{x}{w}\right)^2, \tag{7}$$

$$\chi\left(y\right) \ = \ 0.3\left(1 - 2\frac{y}{h}\right)^2 + 0.44. \tag{8}$$

By inserting (5) and (6) into the ellipsoid equation,

$$\frac{x^2}{(w(y)/2)^2} + \frac{y^2}{(h/2)^2} + \frac{z^2}{p^2(x,y)} = 1 \ \wedge \ z > 0, \tag{9}$$

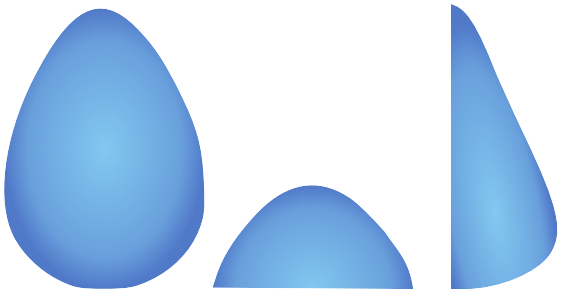

Fig. 9. Coronal, axial and lateral view of an anatomic implant.

we obtain the implicit function describing the surface of the anatomic implants. For the simulation, we again need the projection of implant in dependence of the coordinates x and y, which we obtain by dissolving for z:

$$z\,(x,y) = p(x,y)\sqrt{1 - 4\left(\frac{x}{w(y)}\right)^2 - 4\left(\frac{y}{h}\right)^2}. \qquad (10)$$

VI. Results and Discussion

A. Performance

We have tested our software prototype on a standard desktop PC equipped with an Intel Core 2 Quad Q9450 2.66 GHz processor and 8 GB of RAM. In Table I we provide information on some of the models used and the respective performance achieved. The second column shows the number of tetrahedral elements that are used in the finite element simulation. The next column shows the time required to setup the boundary conditions for the simulation, including the time required to find the implant vertices and elements using the pre-computed kd-tree. Then, we show the time it takes to simulate the deformation induced by the implant using a maximum number of five V(2,1)-cycles of the geometric multigrid solver yielding convergence in all of our examples. Note that in each multigrid V-cycle we perform an update of all element rotations as well as a reassembling of the system of equations to account for the geometric non-linearities of the corotational formulation. The iterative solver allows us to give visual updates after each single multigrid V-cycle. Note that interactions are also possible before the solver is fully converged, in which case the boundary conditions are seamlessly updated to the new implant parameters. Therefore, we achieve an higher update rate of the system. The last column contains the overall update rate one achieves if moving the implant or changing size and volume of the implant.

TABLE I
PERFORMANCE ANALYSIS. ALL OF THE EXAMPLE ARE BASED ON NON-NESTED GRID HIERARCHIES WITH 3 LEVELS, AND 5 MULTIGRID V-CYCLES, EACH INCLUDING AN UPDATE OF THE ELEMENT ROTATIONS, HAVE BEEN PERFORMED. NOTE THAT OUR PROTOTYPE GIVES VISUAL FEEDBACK (AND ALLOWS FOR ADAPTION OF THE IMPLANT PARAMETERS) AFTER EACH MULTIGRID V-CYCLE, YIELDING A 5 TIMES HIGHER UPDATE RATE.

Model	#Elements	Implant Setup	Simulation	Update rate
Mesh1	15K	1ms	125ms	38 Hz
Mesh2	40K	3ms	287ms	16 Hz
Mesh3	60K	8ms	452ms	10 Hz

B. Interaction

As can be seen from Table I, our approach allows for the interactive change of implant position and parameters. This means that the surgeon can interactively adjust the implant extensions, i.e. width, height, and projection (and thereby volume), and can immediately observe the visual outcome of the simulation. As a consequence, the surgeon does not need to inspect the shape of the implants, but can focus on the shape of the patients breast after simulation. Moreover, the implant can be intuitively repositioned in the breast by using buttons such as move left/right/up/down/front/back, and again the simulation results are immediately available (see Figure 10). Movements in depth are realized by moving the surface where the implant is positioned at. If the results are visually pleasant, the prototype can suggest an implant from a given database which matches best the parameters interactively set.

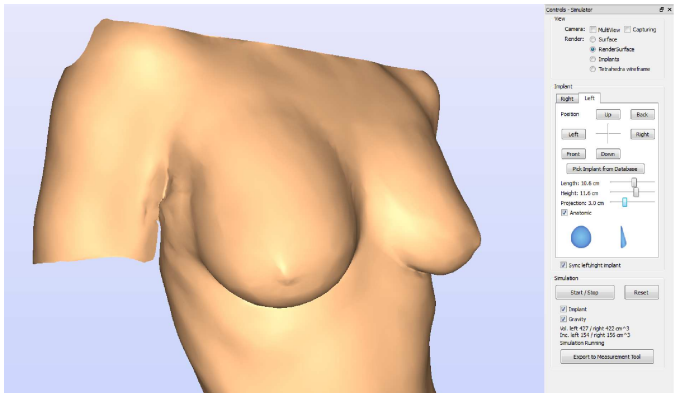

Fig. 10. The graphical user interface of the implant simulation. Immediate visual feedback of the expected outcome is given by the simulation.

On the other hand, the software prototype supports setting the implant parameters automatically by selecting a vendor-specific implant and thus to inspect the visual outcome of this specific implant. A potential workflow could then be to go through a list of available or preferred implants and inspect the results, where the surgeon can still change the position of the implant.

C. Assessment

The developed software prototype contains a large range of automatic assessment tools. Since the landmarks are set for every data-set in the workflow, the tool automatically measures distances (Euclidean and on-surface) between these landmarks. Moreover, since the movement of the landmarks due to the simulation is computed too, one can also obtain these measurements for the simulated, post-operative breasts and thus can directly compare the measurements.

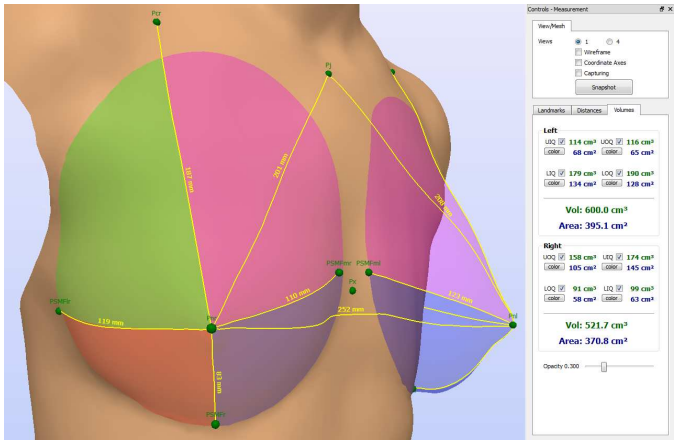

Fig. 11. The breast volume as well as the volumes of the four quadrants are automatically measured by the proposed software prototype. These information can be directly used to support generation of reports of the cases.

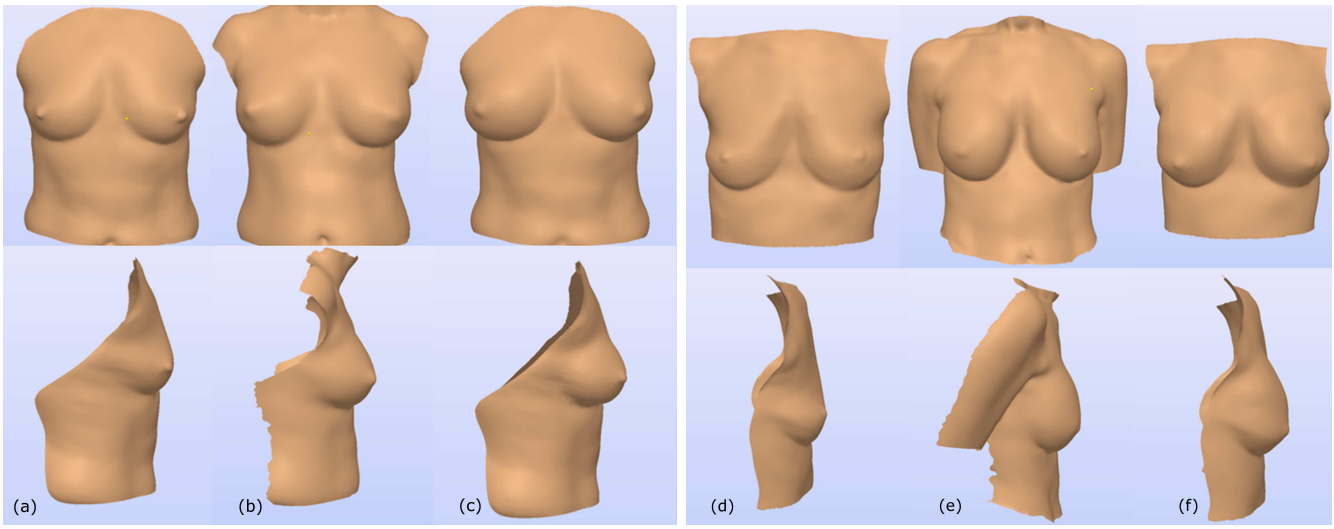

Fig. 12. Retrospective surgical planning for two patients undergoing bilateral subglandular breast augmentation with round implants for patient A (a-c) and anatomic implants for patient B (d-f). From left to right, the frontal (above) and side views (below) of the pre-operative (a + d) and post-operative (b + e) 3D surface scans as well as the simulated results (c + f) are shown for the both patients.

Besides distance measurements we also integrated volume measurements of the whole breast as well as the four breast quadrants, which are automatically determined from the on-surface lines between Pnr and PSMFlr, PSMFmr, Pcr, and PSMFR as is shown in Figure 11.

Additionally, we have integrated tools for comparative assessments, e.g. pre-operative to post-operative comparisons which include, beside distance and volume measurements the direct visualization of surface distances. This can be used both for simulated as well as measured post-operative scans. Please note that for measured post-operative scans, the anatomical landmarks have to be set manually, while they are automatically computed for simulated post-operative results.

All this information can be used to support the surgeon in generation of reports for the cases, which also include screenshots of common views of the breast.

D. Clinical Application for Breast Augmentation Planning

In order to evaluate the clinical reliability and applicability of the presented simulation approach for round and anatomic implants, retrospective simulations for two patients using the known implant shape and volume were performed and the simulation result were compared with the real post-operative 3D surface scan acquired 6 months after surgery (Fig. 12 and 13). The pre-operative surface scans of the two patients (n = 4 breasts) undergoing bilateral sublandular augmentation mammaplasty with round and anatomic implants, respectively, were converted into volumetric finite element breast models by one observer according to the previously described procedure. This task has been performed by a surgeon and took less than 5 minutes per patient. The most clinical relevant bilateral distance measurements between specific landmarks (sternal notch to nipple distance: Pj-Pnl and Pj-Pnr; nipple to submammary fold distance: Pnl-PSMFl and Pnr-PSMFr) and breast volume calculations were compared between the simulated and the actual post-operative 3D scan. Furthermore, the real post-operative 3D models (reference object) were superimposed over the simulated 3D scan (test object) and the breast contour deviation [23], [43] between the two 3D models were quantified by calculating the node to surface root mean square integration of the Haussdorff distance in mm.

The first patient (A) is a 20-year old female (BMI = 20.8) undergoing bilateral subglandular breast augmentation with identical round implants (diameter: $11.5\,$cm; projection: $3.3\,$cm; volume: $250\,\text{cm}^3$) showed a post-operative sternal notch to nipple distance of $23.1\,$cm on the right and $23.0\,$cm on the left, a nipple to submammary fold distance of $8.6\,$cm on the right and $8.7\,$cm on the left and a breast volume of $574\,\text{cm}^3$ on the right and $579\,\text{cm}^3$ on the left. The breast augmentation simulation with the above implant parameters result in a virtual sternal notch to nipple distance of $23.4\,$cm on the right and $23.3\,$cm on the left, a nipple to submammary fold distance of $8.8\,$cm on the right and $8.9\,$cm on the left and a breast volume of $580\,\text{cm}^3$ on the right and $586\,\text{cm}^3$ on the left. In addition, the breast contour deviation analysis between the simulated and the real 3D model showed a root-mean-square value of $3.3\,$mm (Fig. 13 left).

The second 32-year old female patient (B) presented for bilateral subglandular augmentation mammaplasty with identical anatomic implants (width: $12.0\,$cm; height: $11.3\,$cm; projection: $4.2\,$cm; volume: $280\,\text{cm}^3$). The patient had a post-operative sternal notch to nipple distance of $23.3\,$cm on both sides, a nipple to submammary fold distance of $9.0\,$cm on the right and $8.8\,$cm on the left and showing a right breast volume of $620\,\text{cm}^3$ and $616\,\text{cm}^3$ on the left. The retrospective breast enhancement simulation applying the above implant parameters revealed a virtual sternal notch to nipple distance of $23.5\,$cm on the right and $23.6\,$cm on the left, a right nipple to submammary fold distance of $9.2\,$cm and of $9.0\,$cm on the left and a right breast volume of $624\,\text{cm}^3$ and $621\,\text{cm}^3$ on the left. The breast contour deviation analysis showed a root-mean-square value of $2.1\,$mm (Fig. 13 right). Both simulation

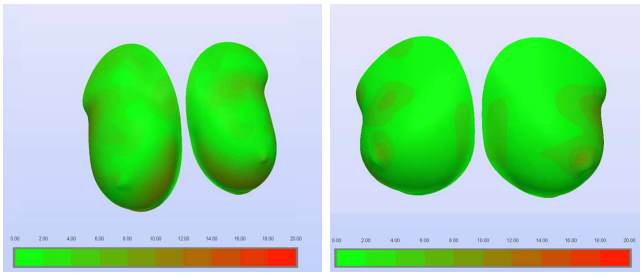

Fig. 13. Comparison of simulated and post-operatively assessed breast shapes for patient A (left) and B (right). The measured root-mean-square distances were 3.3 mm and 2.1 mm, respectively.

results presented no substantial postoperative asymmetries and clinically relevant differences to the actual 3D scan after surgery.

VII. Discussion and Conclusion

In recent years, 3D computer-assisted technologies have gained acceptance in the field of aesthetic breast surgery to optimize surgical planning and outcome analysis based on 3D surface imaging techniques [23], [24], [25], [26]. Nevertheless, a considerable demand for clinical reliable, objective computer-assisted devices which allows pre-operative prediction of the aspired surgical result taking the the biomechanical soft-tissue behaviour into account still remains [30], [31], [32], [33].

The 3D surface imaging device used in our study was a 3D surface laser scanner, a class 1 (for US) and class 2 (for Europe) according to DIN VDE 0837 and IEC Publication 60825-1 with a spectral range of 690 nm and therefore also with no damage to the eye within exposure times up to 0.25 seconds. However, we recommend all patients to close their eyes during the examination since the average acquisition will take approximately 1 second. Nevertheless, the proposed software prototype can be used with other imaging devices such as stereophotogrammetry or fringe light projection as well. However, in our preliminary studies no 3D surface imaging system, respectively no underlying technology proved to have a clear advantage over the other [44], [45].

Recently, commercially available 3D devices also enable the surgeon to model the pre-operative 3D surface image by choosing varying implant sizes and implant contours [45], [46]. But these solutions apply a non-physical morphing approach, and the studies suffer from a lack of sufficient clinical validation as the results are either compared to postoperative scans 6 weeks after surgery [46] or breast surface morphing starts from the 3D surface image solely without taking the thoracic wall as the correct anatomical rear boundary into account [46], [47]. As we have demonstrated in a previous study, changes in breast contour and volume after augmentation mammaplasty caused by postoperative soft tissue swelling are completed not earlier than after 3 months [23]. As actual techniques in aesthetic breast enhancement planning are cumbersome and inaccurate, the presented approach has clear advantages compared to conventional and current available methods.

The study presented a 3D computational tool for aesthetic breast augmentation surgery planning and provides surgeons to prospectively predict breast shape changes and to objectively compare the simulation results of different surgical procedures and varying implants with the real surgical outcome. The 3D breast augmentation surgery simulation tool is based on physical soft tissue properties and implant dimensions, and the prosthesis chest wall position is taken into consideration. Simulations are planned on individual, non-invasive 3D patient data, taking a non-deformed breast surface as a starting point overcoming 2D photo reconstructions and invasive tomography imaging [32], [33]. In addition, not only the post-operative volume change can be predicted with the presented method, also the breast contour changes after surgery will be visualized. The developed surgical planning tool may also serve as a consultation platform to improve the patient-physician consultation and the intra-operative process.

Although our study is the first to present a patient-specific finite element based simulation approach for aesthetic breast augmentation based on 3D surface scans solely, the presented approach is still clinically limited to some degree. Especially the placement of the implant on a surface derived from the fill-in requires further clinical validation. The curvature filled rear breast wall (Figure 4(c)) is shifted towards the back to create the surface where the implant is placed (Figure 6). This approach includes several unknown variables. First, is the resulting implant surface curvature and position in accordance with the real anatomical structures? Second, what is the influence of the breast muscles (major and minor pectoral muscle) to the simulation result as in some augmentation procedures the implant will be placed either under or in front of the muscles? Furthermore, the proposed simulation process does not consider age dependent alterations of skin elasticity and the underlying soft tissue. However, future work might focus on customized patient-specific planning tools using the soft tissue material parameters of the patient by simply applying a pinch test and correlate it to the best matching finite element material model. Additionally, simulation result are dependent on the size of the pre-operative breast, the degree of ptosis and the interaction between the overlying soft tissue and the implants. Especially, the implant surface (smooth or textured) and contour (anatomic or round) might play a role when simulating the resulting breast deformations.

Therefore, future studies are designed to analyze the anatomical agreement between the virtual rear demarcation and the real thoracic wall as well as the breast muscles. The planned study aims to create a 3D breast model for breast augmentation simulation with a rear demarcation of the thoracic wall based solely on 3D surface imaging of 25 young, healthy and non-operated test persons and to anatomically verify this 3D breast model by comparing it with the real anatomical structures using the corresponding MR images of the same subjects. Our previous studies already showed a valuable agreement between the proposed filling of the rear breast wall for breast volume calculations with the 3D reconstructed anatomical thoracic wall based on MRI [17], [18]. The planned MRI study will provide anatomical data of a representative study group that might allow optimizing the parameters used to

determine the implant surface as well as deliver a mean breast muscle geometry, which can be integrated into the software for future simulations of subpectoral and subglandular implant positioning.

The first clinical applications for subglandular implant positioning using the presented software prototype are promising (Figure 12 and 13), but further more detailed validations are needed before a wider clinical application can take place. The surgeons performing the first simulations positively emphasize the clarity and simplicity of the software design and the proposed workflow which enhance the user friendliness (Figure 10). Furthermore the surgeons highlighted the usefulness to interact with the 3D breast model in real time and to see the applied deformations immediately which allows him to compare different types of implants directly during the same evaluation without time consuming interactions. In addition, the surgeons are very pleased by the implemented assessment tools which enable the user to quantify and visualize the performed breast shape changes and to summarize these evaluations in a written report which may contribute to a standardized quality assurance in aesthetic and reconstructive breast surgery in the near future. Finally, to achieve successful and aesthetically pleasing surgical results, breast surgery planning based on a patient-specific 3D surface scan breast model with a reliable quantitative surgical outcome prediction and post-operative 3D breast contour assessment may add a considerable value to aesthetic breast surgery. We believe that a 3D patient-specific physics-based breast augmentation planning tool may play an important role in plastic, reconstructive and aesthetic breast surgery, but will never completely replace the surgeons clinical experience.

Conflict of Interests

All authors disclose any financial or commercial associations and personal relationships with other people, organizations or with the companies named in the study that inappropriately influence (bias) their work or create a conflict of interest with information presented in the submitted study. None of the authors are shareholders of one of the named companies which hard- and software products were used in the study.

Acknowledgements

The authors would like to thank Prof. Dr. rer. nat. Univ. A. Haase, Director of the Zentralinstitut für Medizintechnik (IMETUM), Technische Universität München, Germany for his cooperation and infrastructural support. In addition, we would like to thank Prof. Dr. H.-G. Machens, Director of the Department of Plastic Surgery and Hand Surgery, Klinikum rechts der Isar, Technische Universität München, Germany for his continuous support of our projects which has enabled this study. Funding for the study was received by the Federal Ministry of Economics and Technology (BMWi), Germany.

References

[1] R. Rohrich, “The increasing popularity of cosmetic surgery procedures: a look at statistics in plastic surgery,” *Plast Reconstr Surg*, vol. 106, pp. 1363–1365, 2000.

[2] American Society of Plastic Surgeons, National Cosmetic Procedures. Available at http://www.plasticsurgery.org/Documents/news-resources/statistics/2011-statisticss/2011-cosmetic-procedures-trends-statistics.pdf. Accessed Aug 31, 2012.

[3] M. Ferreira, “Evaluation of results in aesthetic plastic surgery: preliminary observations on mammaplasty,” *Plast Reconstr Surg*, vol. 106, pp. 1630–1635, 2000.

[4] O. M. Tepper, J. G. Unger, K. H. Small, D. B. Feldman, N. Kumar, M. Choi, and N. S. Karp, “Mammometrics: the standardization of aesthetic and reconstructive breast surgery,” *Plast Reconstr Surg*, vol. 125, pp. 393–400, 2010.

[5] J. Chavoin, A. Teysseyre, and J. Grolleau, ““morphobreast”: patient’s data bank management for objective selection of implant’s volume in hypotrophic breasts,” *Ann Chir Plast Esthet*, vol. 50, pp. 487–493, 2005.

[6] M. Westreich, “Anthropomorphic breast measurement: protocol and results in 50 women with aesthetically perfect breasts and clinical application,” *Plast Reconstr Surg*, vol. 100, pp. 468–479, 1997.

[7] F. Bouman, “Volumetric measurement of the human breast and breast tissue before and during mammaplasty,” *Br J Plast Surg*, vol. 23, pp. 263–264, 1970.

[8] B. Campaigne, V. Katch, P. Freedson, S. Sady, and F. Katch, “Measurement of breast volume in females: description of a reliable method,” *Ann Hum Biol*, vol. 6, pp. 363–367, 1979.

[9] C. Kalbhen, J. McGill, P. Fendley, K. Corrigan, and J. Angelats, “Mammographic determination of breast volume: comparing different methods,” *Am J Roentgenol*, vol. 173, pp. 1643–1649, 1999.

[10] R. Rudolph and N. Forcier, “Calculation of silicone breast implant volumes using breast magnetic resonance imaging,” *Aesthet Surg J.*, vol. 29, pp. 310–313, 2009.

[11] A. Pozzobon, M. Sabino Neto, D. Veiga, L. Abla, J. Pereira, T. Biasi, L. Ferreira, L. Yamashita, F. Kawano, E. Nakano, and D. Shigueoka, “Magnetic resonance images and linear measurements in the surgical treatment of breast asymmetry,” *Aesthetic Plast Surg*, vol. 33, pp. 196–203, 2009.

[12] T. Kirianoff, “Volume measurements of unequal breasts,” *Plast Reconstr Surg*, vol. 54, p. 616, 1974.

[13] A. Grossman and L. Roudner, “A simple means for accurate breast volume determination,” *Plast Reconst. Surg*, vol. 66, pp. 851–852, 1980.

[14] G. Brody, “Breast implant size selection and patient satisfaction,” *Plast Reconstr Surg*, vol. 68, pp. 611–613, 1981.

[15] N. Bulstrode, E. Bellamy, and S. Shrotria, “Breast volume assessment: comparing five different techniques,” *Breast*, vol. 10, pp. 117–123, 2001.

[16] L. Kovacs, M. Eder, R. Hollweck, A. Zimmermann, M. Settles, A. Schneider, M. Endlich, A. Mueller, K. Schwenzer-Zimmerer, N. Papadopulos, and E. Biemer, “Comparison between breast volume measurement using 3D surface imaging and classical techniques,” *Breast*, vol. 16, pp. 137–145, 2007.

[17] L. Kovacs, M. Eder, R. Hollweck, and et al., “New aspects of breast volume measurement using 3-dimensional surface imaging,” *Ann Plast Surg*, vol. 57, pp. 602–610, 2006.

[18] M. Eder, A. Schneider, H. Feussner, A. Zimmermann, C. Höhnke, N. Papadopulos, and L. Kovacs, “Breast volume assessment based on 3D surface geometry: verification of the method using mr imaging,” *Biomed Tech*, vol. 53, pp. 112–121, 2008.

[19] M. Eder and L. Kovacs, “Commentary on the article of herold et al.: The use of mamma mri volumetry to evaluate the rates of fat survival after autologous lipotransfer,” *Handchir Mikrochir Plast Chir*, vol. 42, pp. 135–136, 2010.

[20] M. Eder, N. Papadopulos, and L. Kovacs, “Re: Virtual 3-dimensional modeling as a valuable adjunct to aesthetic and reconstructive breast surgery,” *Am J Surg*, vol. 194, pp. 563–565, 2007.

[21] L. Kovacs, M. Eder, N. Papadopulos, and E. Biemer, “Validating 3-dimensional imaging of the breast,” *Ann Plast Surg*, vol. 55, pp. 695–696, 2005.

[22] A. del Palomar, B. Calvo, J. Herrero, J. López, and M. Doblaré, “A finite element model to accurately predict real deformations of the breast,” *Med Eng Phys*, vol. 30, no. 9, pp. 1089–1097, 2008.

[23] M. Eder, F. v Waldenfels, M. Sichtermann, T. Schuster, N. Papadopulos, H. Machens, E. Biemer, and L. Kovacs, “Three-dimensional evaluation of breast contour and volume changes following subpectoral augmentation mammaplasty over 6 months,” *J Plast Reconstr Aesthet Surg*, vol. 64, pp. 1152–1160, 2011.

[24] L. Kovacs, M. Eder, A. Zimmermann, D. Müller, T. Schuster, N. Papadopulos, E. Biemer, M. Klöppel, and H. Machens, “Three-dimensional evaluation of breast augmentation and the influence of anatomic and round implants on operative breast shape changes,” *Aesthetic Plast Surg.*, vol. 36, pp. 879–887, 2012.

[25] O. Tepper, K. Small, J. Unger, D. Feldman, N. Kumar, M. Choi, and N. Karp, "3d analysis of breast augmentation defines operative changes and their relationship to implant dimensions," *Ann Plast Surg*, vol. 62, pp. 570–575, 2009.
[26] D. Esme, A. Bucksch, and W. Beekman, "Three-dimensional laser imaging as a valuable tool for specifying changes in breast shape after augmentation mammaplasty," *Aesthetic Plast Surg*, vol. 33, pp. 191–195, 2009.
[27] D. Chen, D. Chittajallu, G. Passalis, and I. Kakadiaris, "Computational tools for quantitative breast morphometry based on 3d scans," *Ann Biomed Eng*, vol. 38, no. 5, pp. 1703–1718, 2010.
[28] H. Seo, F. Cordier, and K. Hong, "A breast modeler based on analysis of breast scans," *Comp. Anim. Virtual Worlds*, vol. 18, pp. 141–151, 2007.
[29] L. Kovacs, M. Eder, A. Müller, M. Endlich, N. Papadopulos, and E. Biemer, "Three-dimensional computer-assisted intuitive breast surgery planning," *Journal of Biomechanics*, vol. 39, no. Suppl. 1, p. S575, 2006.
[30] E. Gladilin, B. Gabrielova, P. Montemurro, and P. Hedén, "Customized planning of augmentation mammaplasty with silicon implants using three-dimensional optical body scans and biomechanical modeling of soft tissue outcome," *Aesthetic Plast Surg*, vol. 35, no. 4, pp. 494–501, 2011.
[31] L. Roose, W. de Maerteleire, W. Mollemans, F. Maes, and P. Suetens, "Simulation of soft-tissue deformations for breast augmentation planning," *Lecture Notes in Computer Science: Biomedical Simulation*, vol. 4072, pp. 197–205, 2006.
[32] P. de Heras Ciechomski, M. Constantinescu, J. Garcia, R. Olariu, I. Dindoyal, S. Le Huu, and M. Reyes, "Development and implementation of a web-enabled 3d consultation tool for breast augmentation surgery based on 3d-image reconstruction of 2d pictures," *J Med Internet Res*, vol. 14, no. 1, p. e21, 2012.
[33] A. Lapuebla-Ferri, A. del Palomar, J. Herrero, and A. Jiminez-Mocholi, "A patient-specific FE-based methodology to simulate prosthesis insertion during an augmentation mammoplasty," *Medical Engineering & Physics*, vol. 33, no. 9, pp. 1094–1102, 2011.
[34] J. Georgii and R. Westermann, "Corotated finite elements made fast and stable," in *Proc. of the 5th Workshop On Virtual Reality Interaction and Physical Simulation*, 2008, pp. 11–19.
[35] ——, "A streaming approach for sparse matrix products and its application in galerkin multigrid methods," *Electronic Transactions on Numerical Analysis*, vol. 37, pp. 263–275, 2010.
[36] L. Kovacs, A. Yassouridis, A. Zimmermann, G. Brockmann, A. Wöhnl, M. Blaschke, M. Eder, K. Schwenzer-Zimmerer, R. Rosenberg, N. Papadopulos, and E. Biemer, "Optimization of 3-dimensional imaging of the breast region with 3-dimensional laser scanners," *Ann Plast Surg.*, vol. 56, no. 3, pp. 229–36, 2006.
[37] H. Si, "TetGen, a quality tetrahedral mesh generator and three-dimensional delaunay triangulator, v1.3 user's manual," Weierstrass Institute for Applied Analysis and Stochastics, Berlin, Tech. Rep. 9, 2004.
[38] M. Bro-Nielsen and S. Cotin, "Real-time volumetric deformable models for surgery simulation using finite elements and condensation," in *Proceedings of Eurographics*, 1996, pp. 57–66.
[39] K.-J. Bathe, *Finite Element Procedures*. Prentice Hall, 2002.
[40] C. Rankin and F. Brogan, "An element-independent co-rotational procedure for the treatment of large rotations," *ASME J. Pressure Vessel Tchn.*, vol. 108, pp. 165–174, 1986.
[41] J. Georgii and R. Westermann, "A Multigrid Framework for Real-Time Simulation of Deformable Bodies," *Computer & Graphics*, vol. 30, pp. 408–415, 2006.
[42] J. Georgii, D. Lagler, C. Dick, and R. Westermann, "Interactive deformations with multigrid skeletal constraints," in *Proceedings of the 7th Workshop On Virtual Reality Interaction and Physical Simulation*, 2010, pp. 39–47.
[43] M. Eder, F. Waldenfels, A. Swobodnik, M. Klöppel, A. Pape, T. Schuster, S. Raith, E. Kitzler, N. Papadopulos, H. Machens, and L. Kovacs, "Objective breast symmetry evaluation using 3-d surface imaging," *Breast*, vol. 21, no. 2, pp. 152–158, 2012.
[44] M. Eder, G. Brockmann, A. Zimmermann, M. Papadopoulos, K. Schwenzer-Zimmerer, H. Zeilhofer, R. Sader, N. Papadopulos, and L. Kovacs, "Evaluation of precision and accuracy assessment of different 3-d surface imaging systems for biomedical purposes," *J Digit Imaging*, vol. 26, no. 2, pp. 163–172, 2013.
[45] P. Patete, M. Eder, S. Raith, A. Volf, L. Kovacs, and G. Baroni, "Comparative assessment of 3d surface scanning systems in breast plastic and reconstructive surgery," *Surg Innov.*, vol. 20, no. 5, pp. 509–515, 2013.
[46] B. Mailey, A. Freel, R. Wong, D. Pointer, and K. Khoobehi, "Clinical accuracy and reproducibility of portrait 3d surgical simulation platform in breast augmentation," *Aesthet Surg J.*, vol. 33, no. 1, pp. 84–92, 2013.
[47] C. Creasman, D. Mordaunt, T. Liolios, C. Chiu, A. Gabriel, and G. Maxwell, "Four-dimensional breast imaging, part ii: clinical implementation and validation of a computer imaging system for breast augmentation planning," *Aesthet Surg J.*, vol. 31, no. 8, pp. 925–938, 2011.